Received: 8 July 2020 | Revised: 16 October 2020 | Accepted: 30 October 2020

DOI: 10.1002/nano.202000060

RESEARCH ARTICLE

Nano Select WILEY

Low-dose liquid cell electron microscopy investigation of the complex etching mechanism of rod-shaped silica colloids

Sina Sadighikia | Albert Grau-Carbonell | Tom A.J. Welling | Ramakrishna Kotni | Fabian Hagemans | Arnout Imhof | Marijn A. van Huis | Alfons van Blaaderen

Soft Condensed Matter, Debye Institute for Nanomaterials Science, Utrecht University, Princetonplein 5, Utrecht 3584CC, The Netherlands

Correspondence
Marijn Arnout van Huis, Soft Condensed Matter, Debye Institute for Nanomaterials Science, Utrecht University, 3584 CC Utrecht, The Netherlands.
Email: m.a.vanhuis@uu.nl

Abstract

Understanding the chemical structure of rod-shaped silica colloidal particles is attainable by investigating their etching mechanism in solution. Liquid Cell (Scanning) Transmission Electron Microscopy (LC-(S)TEM) is a promising technique through which the etching of these particles can be observed in real time, and at the single particle level, without possible deformations induced by the surface tension of dried particles. However, the presence of high energy electrons, and the different geometry in LC experiments may alter the conditions of in situ experiments compared to their ex situ counterparts. Here we present a controlled low-dose LC-STEM study of the basic etching process of micron-sized silica rods that are immobilized on the SiN window of a liquid cell. The results show that using low-dose imaging conditions, combined with a low accumulated electron dose, and optimized flow rates of solutions allow for investigation of the chemical etching mechanism of silica colloidal particles using the LC-(S)TEM technique with negligible effects of the electron beam. A comparison of ex situ etching experiments with LC-STEM observations show that the LC geometry can play a crucial role in LC-STEM experiments where the diffusion of the etching particles is important, which should be considered during the interpretations of LC-STEM results.

KEYWORDS

anisotropic particles, etching, liquid cell electron microscopy, silica

1 | INTRODUCTION

The widespread application of anisotropic colloidal particles in the self-assembly of new materials is driven, among others, by the ability of such systems to form colloidal liquid crystal phases. Due to the great potential of anisotropic particles in chemical, electrical, and optical applications, they have attracted much attention.[1–9] New complex functional materials are achievable by self-assembly of these colloidal building blocks.[10–12] Colloidal silica particles are also of interest because of their use in physico-chemical studies of colloidal model systems.

The ease of chemical modification of colloidal silica particles' surfaces by using various types of functional groups, allows for making a vast range of silica particles with different functionalities and interparticle interactions.[13–15] The recently developed model system of (fluorescent) silica rods by Kuijk et al.[16] is a powerful model system to study their self-assembly into various liquid crystalline phases in real space.[13,16–18] The synthesis procedure of these rod-shaped silica particles is a simple one-pot synthesis in which ethanol, water, sodium citrate, and ammonia, are mixed with a solution of polyvinylpyrrolidone (PVP) in 1-pentanol to arrive at a dispersion of water with dissolved ammonia, PVP and citrate. Silica rods start to grow upon the addition of the strongly apolar tetraethyl orthosilicate (TEOS) to the pentanol oil phase. The growth of these rods takes place from the water-in-oil emulsion droplet and starts with deposition of silica on the oil–water interface after which the rod grows from silica deposited from the watery droplet attached to the growing end of the rods. This growth mechanism results in an anisotropic bullet shaped particle with a flat end where the watery droplet was attached and a rounded tip due to the anisotropic supply of hydrolyzed TEOS.[13,15] Although the synthesis of these rod-shaped particles has been studied extensively, there are few studies on their chemical composition. Recently, it has been revealed that these rod-shaped silica particles can be transformed into a cone-shaped colloidal silica particles upon mild etching by NaOH in water.[19] Understanding the chemical structure of these particles is key to reveal the mechanism of this transformation, which also opens the way to obtain other novel particle shapes.

In order to obtain a fundamental understanding of the etching process of rod-shaped silica particles at the single particle level, we have taken a direct approach of imaging this process in situ using Liquid Cell Scanning Transmission Electron Microscopy (LC-STEM).[20–22] In this research we wanted to determine if LC-(S)TEM could be used as a technique to study the chemical composition of these rod-shaped silica particles by monitoring their etching mechanism in a basic environment in real time without affecting the process by the observation. However, the presence of high energy electrons as well as the confining geometry of the liquid cell (LC), combined with the fact that only particles stuck to the cell window can be continuously observed in time, could all significantly modify the etching process as compared to etching which takes place while particles are dispersed and undergoing Brownian motion. Furthermore, it is known that the electron beam can affect the imaging area and its surroundings in both direct and indirect ways and chemical reactions could be significantly altered by the electron beam.[23] In order to validate the results in a LC-(S)TEM experiment, we need to control a large number of variables which affect the ongoing chemical and physical processes inside the cell.[24–26] Therefore, for in situ monitoring of a chemical process, we need to minimize the influence of the electron beam, optimize the flow rate of solutions, and understand the effect of the liquid cell geometry. A known effect of electron irradiation is the growth or degradation of nanomaterials induced by reducing or oxidizing environments due to the presence of reactive radicals and molecular species formed by electron–solvent interactions.[23,25,27] So far, by utilizing different solvents and scavengers, the electron beam induced nucleation, growth and degradation of various types of nanomaterials were studied using the LC-(S)TEM technique.[28–43] However, there are few studies on direct monitoring of a chemical reaction with LC-(S)TEM.[44–47] Etching of rod-shaped silica particles is a nice model process for investigating if LC-(S)TEM can be used for in situ monitoring of chemical reactions on colloids. If the effects of the electron beam can be minimized, the etching mechanism and therefore the inhomogeneous chemical composition of these particles can be studied at the single particle level in real time at a high spatial resolution. Importantly, LC-STEM also would get rid of artifacts that can be induced by strong drying forces that occur if particles are dried on TEM grids without lengthy procedures such as supercritical drying.

Rod-shaped silica colloids prepared by ammonia-catalyzed hydrolysis and condensation of tetraethyl orthosilicate in water droplets, containing polyvinylpyrrolidone cross-linked by citrate ions in pentanol, were found to have an inhomogeneous chemical structure both along the length of the particle as in the perpendicular direction along the diameter of the particle.[19] Here, we show that by tuning the pH of the LC solution while the particles are stuck to a SiN window, while continuously flowing NaOH basic solutions through the cell and optimizing the flow rate, together with using low-dose rate imaging conditions (1–10 $e^- nm^{-2} s^{-1}$), direct observation of the silica rods etching mechanism is achievable. Furthermore, using a discontinuous imaging approach by blanking the beam for a certain amount of time between recording the frames, we minimized the accumulated electron dose ($e^- nm^{-2}$) on the particle. The accumulated electron dose is also known to have a great impact on LC-(S)TEM results in certain cases.[48] Comparison with ex situ etching experiments showed that the low electron dose rate in combination with a low total electron dose, which was at least one order of magnitude lower than previous LC-(S)TEM studies, played a significant role in observing the "real" chemical process with negligible effects of the electron beam. However, the effects of the confining geometry of LC in combination with the fact that only particles immobilized on the window were observed, where the Brownian motion of the particles

was completely suppressed, should be taken into account. Altered accessibility and diffusion rates could result in different etching pathways of the particles in comparison to the etching happening to particles that diffuse freely in the reactive solution. Our LC-STEM observations revealed how these rod-shaped silica particles undergo inhomogeneous etching along the length of the rod in an aqueous NaOH solution, and how rods with a certain internal morphology for certain NaOH concentrations finally turned into a cone-shaped silica particle. Further validation of the LC-STEM observations for the etching of rod-shaped silica particles was carried out using even more complex structured segmented silica rods with a known inhomogeneous chemical structure. Here, the degree of condensation along the silica rod was tuned in such a way that a desired segment of the rod had a less condensed silica structure so that faster etching of that segment was expected simply due to the smaller number of siloxane bonds that needed to be broken as compared to the rest of the particle.[49,50] This inhomogeneous silica structure could be obtained during particle synthesis by changing the reaction temperature, precursor concentration, and/or ethanol concentration.[51] Finally we used the information obtained to explore the chemical composition of newly developed, even more complexly structured silica rod-shaped particles known as crooked silica rods. Such crooked rods have been developed recently in our group[52] and that of others[53] as such particles can form interesting new colloidal liquid crystal phases.[54]

2 | RESULTS AND DISCUSSION

Rod-shaped silica particles were synthesized as described by Kuijk et al.[16] (Figure S1). In this process rods grow from a water-in-oil emulsion droplet which is rich in hydrolyzed TEOS, and because of this anisotropic supply of precursor the particle grows from the droplet only in one direction. Since the precursor concentration is highest at the start of the reaction, growth takes place fastest during that stage.[19] The high concentration of the silicon hydrolyzed alkoxide at the beginning of the reaction results in a porous structure by the addition of oligomers near the round tip of the rod, whereas the lower concentration near the end of the growth results in a more densely condensed structure by the addition of monomers.[19,55] Furthermore, in the radial direction the chemical composition is inhomogeneous as well; a low concentration of silicon hydrolyzed alkoxide in the pentanol phase result in the formation of a condensed silica shell around the particle. This shell is thickest for the part that is grown first.[19] Dissolution of silica in alkaline solutions occurs when the hydroxide ion (OH^-) attacks the silicon atom and replaces one of the siloxane bonds in a transition state with coordination number five.[49] In addition, the free energy gain associated with the weakly acidic silanol groups that strongly increases the solubility of silica at pH above ~10. Silica rods are typically stable in water for years. By minimizing the electron beam irradiation effects, we showed that silica rods are stable also during the LC experiments in pure water (see Figure S7 in the Supporting Information).

To better understand the influence of the LC-STEM parameters on our in situ etching experiments, we initially optimized these parameters to the extent where the effects of the electron beam could be neglected by investigating the effects of varying the flow rate, NaOH concentration, and accumulated electron dose on the resulting LC-STEM observations of the etching mechanism of silica rods. Furthermore, we investigated the effect of the liquid cell geometry on the etching mechanism of these rods by performing ex situ counterpart experiments that could be more directly compared to etching experiments inside the LC.

2.1 | Static in situ etching experiments

First, static (without flow through the cell) LC-STEM experiments were performed by dispersing the particles in a 100 mM NaOH aqueous solutions and preparing the liquid cell by drop-casting 2 μL of this solution on the SiN chips. No etching was observed after 60 minutes of continuous imaging at an electron dose rate of 18 $e^- nm^{-2} s^{-1}$ of one particle at this high NaOH concentration (Figure S4). This is surprising, as silica is expected to dissolve at such a high pH. There are two possible causes for this: The sample volume that we used to prepare the liquid cell was quite small (2 μL). It is likely that the solution became immediately saturated with silicate ions due to the presence of a large number of particles in the small volume of the basic solution, and etching did not take place as the pH decreased by the activity of the resulting silanol groups and the solubility limit was already reached. The higher initial concentration of silica particles (350 mM) compared to the NaOH concentration (100 mM) also roughly confirms this assumption. It is noteworthy that decreasing the concentration of the silica rods is only possible to a certain minimum number of particles. Below this concentration we were not able to perform the experiment since in most of the experiments there were no particles on the LC window. By performing the static etching experiment at the lowest possible concentration of particles, we did not observe the etching process. We propose that this minimum concentration of silica particles is still enough to deplete the NaOH ions in the solution since the cell volume is approximately tenth of a micro liter. An other possible explanation is associated with pH changes upon electron beam irradiation

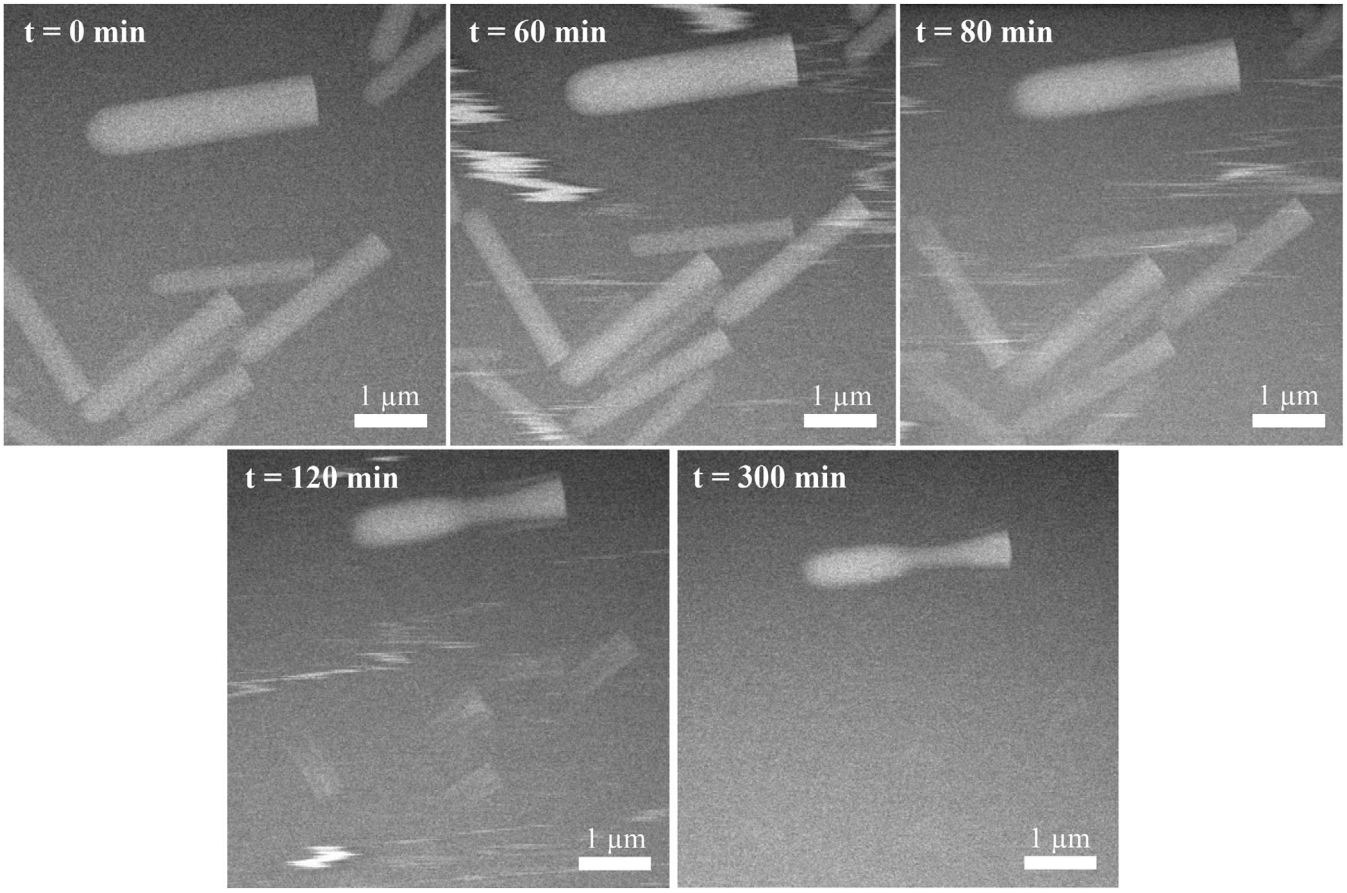

Figure 1 STEM image series showing optimized flow rate of basic solutions in silica rods etching process in real time. The particles were imaged for 6 hours while a 50 mM NaOH solution was flowing through the cell at 0.3 μL min^{-1}. A total number of 94 frames were recorded with an electron dose rate of 7e$^-$ nm^{-2} s^{-1}and a total accumulated electron dose of 1.1×10^4e$^-$ nm^{-2}. Scale bars indicate 1 μm

in LC-(S)TEM experiments. Calculations involving many radiolysis products, which are always made for pure water and do not take the presence of the silica rods into account, indicate that the pH of the solution in the liquid cell drops upon electron beam irradiation, where alkaline solutions are most strongly affected by the electron beam irradiation.[23] Therefore, the pH of the solution could have decreased when it was continuously exposed to the electron beam, thereby inhibiting the etching process. However, the irradiated volume was small compared to the total volume of the liquid cell, and this contribution was most likely small. Unfortunately, measuring the pH of the remaining solution after a static experiment showed to be technically impossible with our current set up. Nevertheless, the LC-STEM observations also showed that some dissolved silica redeposited on the surface of the particle and/or on the SiN window in the field of view. This silica could only have come from the dissolution of some of the rods, which clearly therefore is not always visible by looking at changes of the particle shape. It has been shown that the silica redeposition happens in LC-STEM and that it is strongly related to the electron beam irradiation.[56]

2.2 | Effect of flow rate on in situ LC-STEM etching experiments

The ability to flow NaOH aqueous solutions through the cell, enabled us to overcome several of the issues associated with the previous LC-STEM results by continuously renewing the basic solution in the imaging area. We used a syringe pump to flow the NaOH solutions through the cell at a controlled flow rate within the range of 0.1 to 5 μL min^{-1}. Figure 1 shows a few image series of the etching process of rod-shaped silica particles in time. In a 50 mM NaOH solution the etching process was recorded for 6 hours while the solution was flowing through the cell with a flow rate of 0.3 μL min^{-1}. The observations showed that some particles were passing through the field of view. These particles must have been diffusing inside the cell from the beginning of the experiment and were dragged along by the flow. However, particles that were initially attached to the SiN window remained in the field of view during the complete etching process (6 hours), which enabled us to record the complete etching mechanism of silica rod-shaped particles. We will explain the etching

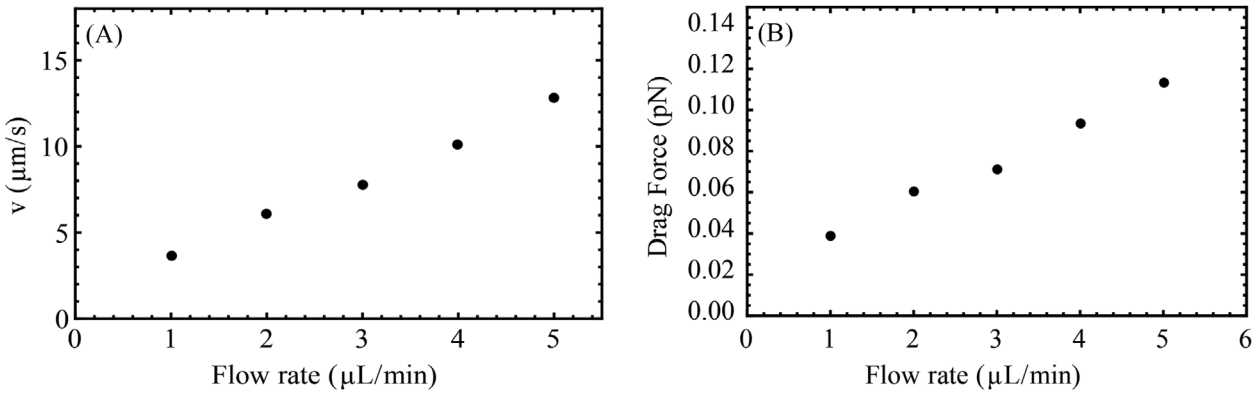

Figure 2 a) The linear relationship between the flow velocity and the flow rate. b) The linear relationship between the drag force on a silica rod-shaped particle with dimensions: L = 2.6 μm D = 300 nm and the flow rate. The drag force on the particle for 5 $\mu L\,min^{-1}$ is three times bigger than the same for $1\mu L\,min^{-1}$

mechanism in the further sections in detail. In order to investigate the effect of the flow rate in our observations, we performed several LC-STEM experiments using different flow rates. Supporting Movie 1 shows a video of a LC-STEM experiment using a flow rate of 5 $\mu L\,min^{-1}$. These observations show particles initially attached to the SiN window detaching from the window and moving out of the field of view 10 minutes after the flow was started. This indicates that a high flow rate can detach the silica rods from the SiN window within a short time, and observation of the full etching process would then not be possible. The NaOH solution slightly etched the particles and made them attach too loosely to the SiN window, and the 5 $\mu L\,min^{-1}$ flow rate was capable of detaching these particles from the window. The role of the base in the detachment was confirmed by a reference experiment, where the same flow rate but with deionized water did not detach particles even after 1 hour of continuous flow. Repeating the experiments with different flow rates revealed that observation of the etching process was feasible within the range of 0.1 to 1 $\mu L\,min^{-1}$.

To better understand the effect of the flow rate on the etching process, the drag force on the silica rod-shaped particles was estimated by measuring the flow velocity in the main channel (window) of the liquid cell. To obtain the flow velocity, another LC-STEM experiment was conducted by flowing 400 nm spherical silica particles through the cell. The cell configuration was the same as used for the etching experiments with silica rod-shaped particles. A diluted sample of silica spheres in deionized water was loaded in the syringe and the flow was started with a flow rate of 5 $\mu L\,min^{-1}$. This experiment was repeated for flow rates of 4, 3, 2, and 1 $\mu L\,min^{-1}$ with the same LC. To increase the accuracy of the experiment, image recording was started 20 minutes after changing the pump speed to stabilize the new flow rate. Sequences of images were recorded with a scanning time of 0.5 second per frame and a total duration of 30 minutes for each flow rate. The image sequences were analyzed by tracking the positions of the particles from image to image (MTrackJ plug-in for Image J (Fiji version)). The trajectories recorded at different pump speeds were analyzed to obtain a relationship between the flow velocity v in the main channel and the flow rate setting on the syringe pump. Results from Figure 2a show that the flow velocity changes linearly with the flow speed setting of the pump. Therefore, for this microfluidic system it can be concluded that the flow velocity was proportional to the pump speed, assuming that the velocity of the particles is a measure of the velocity of the liquid front in the main channel thus neglecting Brownian motion. Knowing the flow velocity, the drag force on the rod-shaped silica particles can be estimated as follows:

$$\vec{F}_{drag} = -\xi\vec{v} \tag{1}$$

where ξ is the drag coefficient of the rods and $\vec{v}$ is the velocity of the particle relative to the flow. ξ can be found from the expression for the translational diffusion coefficient D_t since the diffusion coefficient is equal to $k_BT.\xi^{-1}$. For dilute suspensions, the expression for the translational diffusion coefficient of finite rods, modeled as cylinders, is[57]:

$$D_t = \frac{k_BT\left(ln\left(\frac{L}{D}\right)+\gamma\right)}{3\pi\eta_0 L} \tag{2}$$

where k_BT is the thermal energy, L the total head-to-tail length of the rod, D the diameter, and η_0 the viscosity of the solvent. The factor γ is the so-called end-effect correction which is a function of the rod dimensions[58] and should

be applied when $2 < L/D < 30$:

$$\gamma = 0.312 + 0.565\frac{D}{L} - 0.100\left(\frac{D}{L}\right)^2 \quad (3)$$

If we derive the drag coefficient ξ from Equation 2 and insert it in Equation 1, the drag force for rod-shaped particles can be calculated as follows:

$$\vec{F}_{drag} = -\frac{3\pi\eta_0 L}{ln\left(\frac{L}{D}\right) + \gamma}\vec{v} \quad (4)$$

calculations of drag forces for different flow velocities show that the drag force on the particle increases almost linearly with the flow rate (Figure 2b). Using a 5 μL min^{-1} flow rate the drag force is three times bigger than when using 1 μL min^{-1} which according to the LC-STEM observations was enough to wash all the particles away from the SiN window. The calculations also confirm that the drag force on spherical nanoparticles would be too low to remove them from the SiN window even for the highest flow rate in our system (5 μL min^{-1}). It is noteworthy that Equation 1 does not take into account the hydrodynamic interactions between the particle and the cell wall. However, since the ratio between drag force for different flow rates is of importance in our study, we neglect this interaction, which is assumed to be proportional to the flow rate. During the LC-STEM experiment with silica spheres to calculate the flow rate another interesting observation was made. Particles which were flowed into the cell tended to go out of the window (Figure S5). This was the case for particles which were coming in the SiN window from both the top and the bottom parts. This also happened regardless of the flow rate. This observation is important for the self-assembly experiments via LC-STEM because for these experiments the maximum number of particles is needed in the field of view.

2.3 | Effect of base concentration on in situ etching of silica rods

In order to analyze the dissolution kinetics of silica rod-shaped particles and also the effect of the base concentration on the final shape of the particle, we performed several LC-STEM experiments using three different NaOH concentrations (10, 50, 100 mM) at a fixed flow rate of 0.3 μL min^{-1} and a fixed electron dose rate of 7 e$^-$ nm^{-2} s^{-1} together with a fixed total accumulated electron dose of $\sim$ 1000 e$^-$ nm^{-2}. Since the etching kinetics are strongly size dependent, we analyzed particles with similar particle sizes in each experiment. Figure 3 shows the effect of the three different NaOH concentrations on the etching mechanism and etching kinetics of silica rods. The time at which the etching became visible was different for each of these base concentrations. The first signs of etching, which happened at a region in the middle of the particle but closer to the flat end, was observable after approximately 60 minutes for 100 mM NaOH, observable after about 90 minutes for 50 mM NaOH and after about 120 minutes for 10 mM NaOH. We designate the region of the particle in which the etching started first as the sensitive part of the particle. LC-STEM observations show that initially the etching rate was the highest at this sensitive part of the particle, while it gradually decreased as the etching proceeded in time. This could be due to the presence of a thin silica shell around the particle which has a higher cross-linked SiO_2 structure acting as a protective layer against etching.[19] This thin silica layer forms around the particle by condensation of TEOS from the oil-phase during particle synthesis and is more prominent around the rounded tip of the particle since this part is exposed to the growth solution for a longer time and it stayed attached to the SiN membrane during the whole in situ etching experiment. Furthermore, the flat end of the particle is the most condensed part of the particle due to the slow condensation of silica during the last stages of particle synthesis. Therefore, the LC-STEM observations also suggested that the region in the middle of the particle closer to the flat end was the part of the particle most sensitive to the etchant. The etching process began from this part of the particle and that was the case for all particles with different sizes and for all base concentrations.

2.4 | Etching mechanism of rod-shaped silica particles

Overall, the etching mechanism of rod-shaped silica particles in a confining LC geometry took place in three main steps (Figure 4 and supporting movie 2). By flowing the NaOH aqueous solution into the cell, the etching process started and became observable after a certain period of time for each base concentration at the sensitive part of the particle where the silica shell is the weakest. As was mentioned before, it is likely that some silica was already dissolved without this being visible as a change in morphology and/or density of the particles. This starting region of dissolution was the same for all particles regardless of the size of the particle and the base concentration. Nevertheless, the time when the dissolution started to become visible did depend on the particle size. Next, the etching continued by transport of silica from the inner core through the thin shell at the same region for a while, making this part of the rod thinner in time. Slight etching also happened at the rounded tip and the flat end of the particle; however, the etching rate at these regions was found to

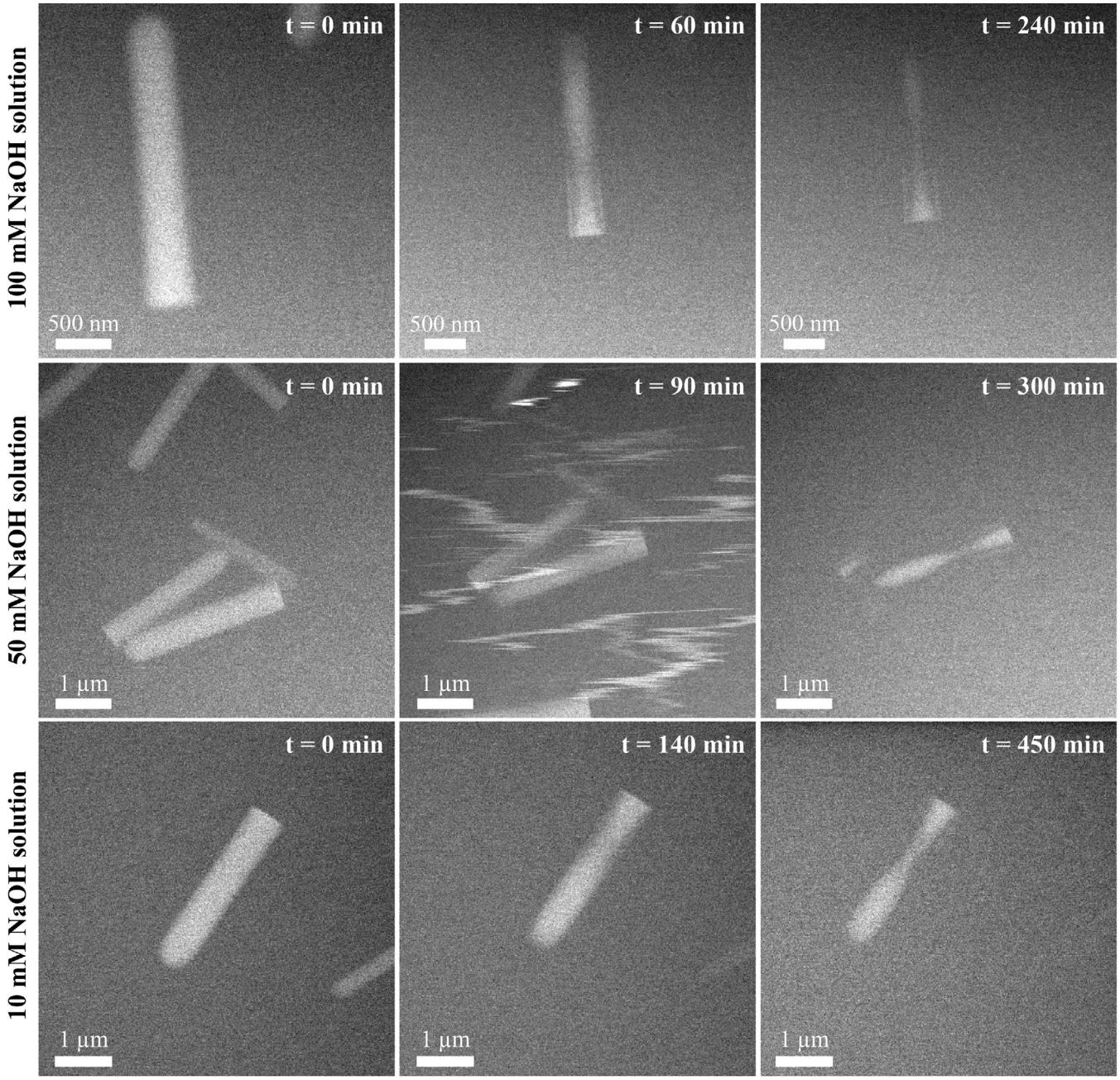

Figure 3 Etching mechanism of silica rods for different concentrations of NaOH solutions. The flow rate was 0.3 $\mu L\ min^{-1}$, the electron dose rate was $7e^{-}\ nm^{-2}\ s^{-1}$, and the total accumulated electron dose was $\sim 1000e^{-}\ nm^{-2}$ for all experiments. The etching process time is different for different base concentrations; however, the etching mechanism is the same.

be significantly lower than the etching rate at the edge of the sensitive part of the particle, due to the stronger shell around the rounded tip of the particle and the more condensed silica at the flat end. Finally, after a longer etching period, necking happened at the sensitive region of the particle, eventually leading to break off. The resulting shape after this step was a cone-shaped silica particle which had a smaller length compared to the initial rod-shaped particle (see also Supporting Movie 2 for a LC-STEM demonstration of the final stage of the etching mechanism). The necking-and-breaking step of the etching process was not previously known from ex situ experiments[19] and it was only revealed during the direct observation of the etching process at a single particle level using LC-STEM.

It is worthwhile to mention that the structural characterization cannot be provided directly as there exists no technique that can probe the degree of condensation on the single particle level. Using NMR it is possible to determine the degree of condensation; however, this will result in an average value over the whole system. As such, we

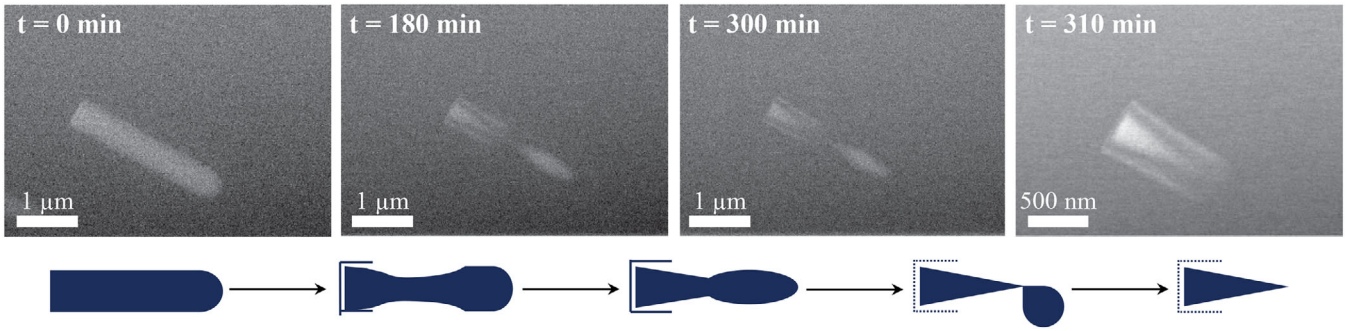

Figure 4 Three step etching mechanism of rod-shaped silica particles attached to the SiN window in basic solutions revealed by LC-STEM experiments (top), and its schematic representation (bottom). In this experiment the NaOH concentration was 100 mM, the flow rate was 0.3 μL min^{-1}, the electron dose rate was 7e$^-$ nm^{-2} s^{-1}, and the total accumulated electron dose was ~1000e$^-$ nm^{-2}.

determined the degree of condensation through an indirect method (etching) at the single particle level in real time to reveal the different degree of condensation through the length and the diameter of the rod.

2.5 | Effect of accumulated electron dose on the etching of silica rods

We also addressed the question concerning the extent to which the observed etching process was influenced by the electron beam irradiation. This influence can be revealed from a change in the etching rate and/or the etching mechanism during the LC-STEM observations. Using a discontinuous imaging approach, we modified the blanking time of the electron beam between recordings of the images of the particles to investigate the accumulated electron dose effects on the etching process. To this end, we exposed particles to electron beam irradiation for different periods of time by recording a different total number of frames for each particle while fixing the electron dose rate at 7e$^-$ nm^{-2} s^{-1} with these imaging conditions: 1024 × 1024 pixels, 24 μs dwell time, and 6.12 nm pixel size. Figure 5 shows image series for four distinct particles imaged with different blanking times during the same LC-STEM experiment. During this experiment a solution of 10 mM NaOH was flowed through the cell at a rate of 0.3 μL min^{-1}. The observations showed that the rate and the mechanism of etching was the same for all particles when they were imaged with low-dose imaging conditions, regardless of the blanking time duration between the recorded images. Furthermore, an overview of the cell after the etching stopped showed that all the particles with similar sizes etched by the same mechanism and at the same rate. This indicates that imaging the etching process of rod-shaped silica particles with low accumulated electron dose did not alter the rate nor the mechanism of the etching process for total doses lower than 3.4×10^4 e$^-$ nm^{-2}, since the accumulated electron dose never reached a threshold with the capability of affecting the chemical process. Using a high electron dose rate (>1000 e$^-$ nm^{-2} s^{-1}) results in a severe shape deformation of the silica rod in the scanning direction (see Figure S8 in the Supporting Information). Therefore, with a negligible effect of electron beam irradiation, investigations of the etching process of this system of particles were successfully achieved.

2.6 | Effect of confining geometry and sticking of particle as opposed to Brownian motion

Finally, ex situ experiments with the same particles and the same etchant were performed in order to compare them with the LC-STEM observations. Two main ex situ experiments were carried on. First, a sample was prepared exactly like the in situ sample preparation: 2 μL of the sample solution was drop-casted on one of the liquid cell chips and let to dry at room temperature to assure that a number of particles were attached to the SiN window. Then these chips were each placed in a plastic bottle filled with 40 mL of aqueous NaOH. 100 mM and 10 mM NaOH solutions were used for these experiments. The vials were left to stand without stirring at room temperature. One sample was retrieved from its solution every 15 minutes for 7 hours after placing the chips in the bottle. For each etching time a separate SiN chip was used in a separate bottle. Next, samples were inspected with STEM using a normal TEM holder. The STEM images confirmed that the mechanism of ex situ etching for the particles that were attached to the SiN window was the same as the in situ etching mechanism where the rod-shaped silica particles turned into cone-shaped silica particles via necking-and-breaking. Figure 6, a and b, show the end result for this ex situ etching experiment (data not shown for each etching time).

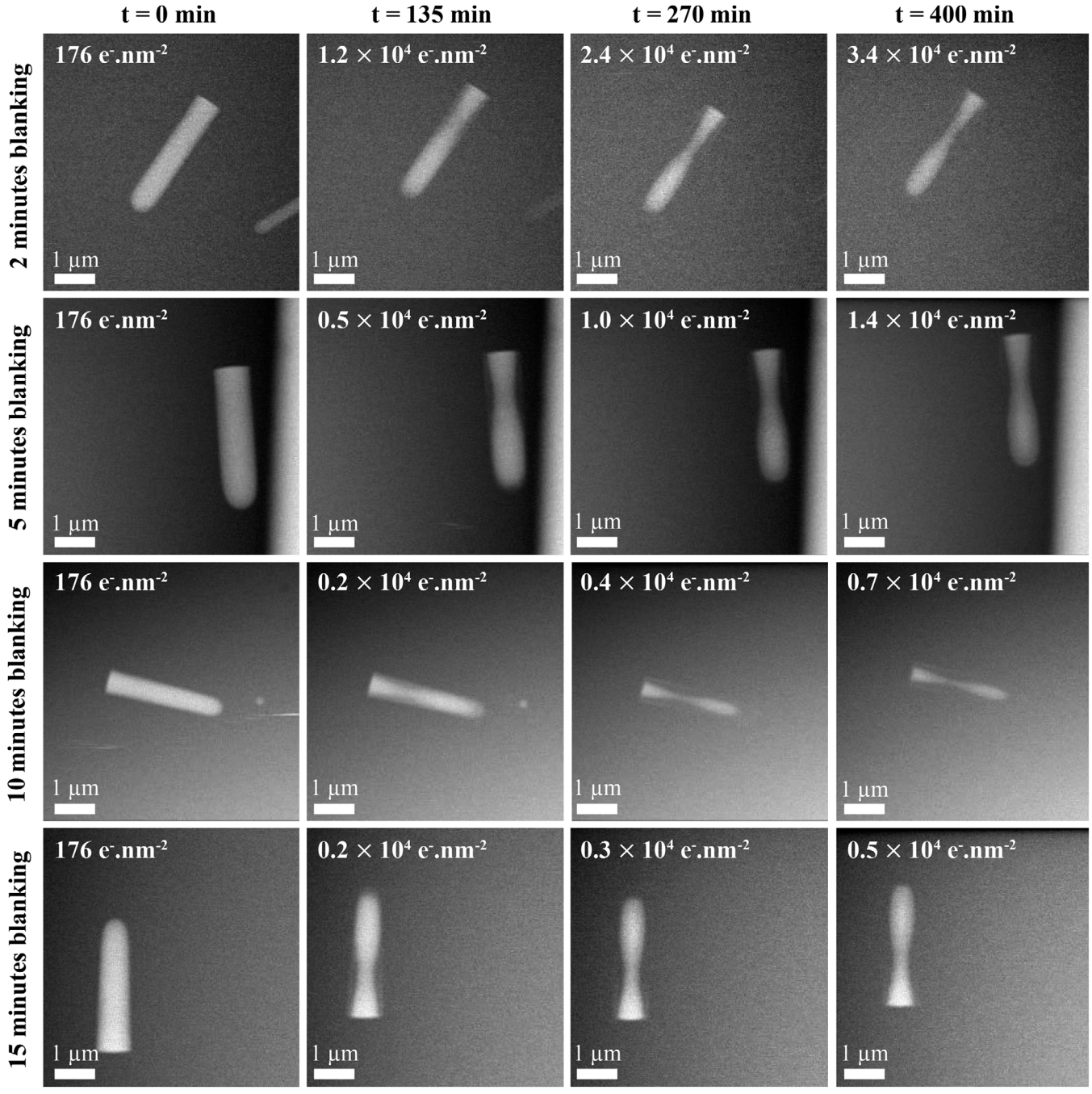

Figure 5 STEM image series of four distinct particles imaged with different beam blanking time indicating different accumulated electron dose (e^{-} nm^{-2}) on each particle. The corresponding total accumulated electron dose is shown on each frame. The scale bar indicates 1 μm.

A second experiment was performed with freely diffusing silica rods, The particles were redispersed in NaOH aqueous solutions. This ex situ etching experiment was performed with 0.5, 3, 10, and 100 mM NaOH concentrations. Samples were collected by dipping a conventional TEM grid in each solution every 15 minutes and were subsequently imaged with STEM. Figure 6, c-f, shows the end product of the etching of rod-shaped silica particles that were freely dispersed during etching, for different base concentrations (data not shown for each etching time). Etching at low base concentrations (0.5 mM) showed the same mechanism as the LC observations for etching of these particles. However, at higher base concentrations such as 10 and 100 mM NaOH the etching mechanism/product was different from the mechanism observed in the LC experiments. The STEM images show that the particles dispersed in higher base concentrations turned into sharper cone-shaped silica particles with a larger length, indicating that the etching also occurred at the tip of these particles and the necking-and-breaking

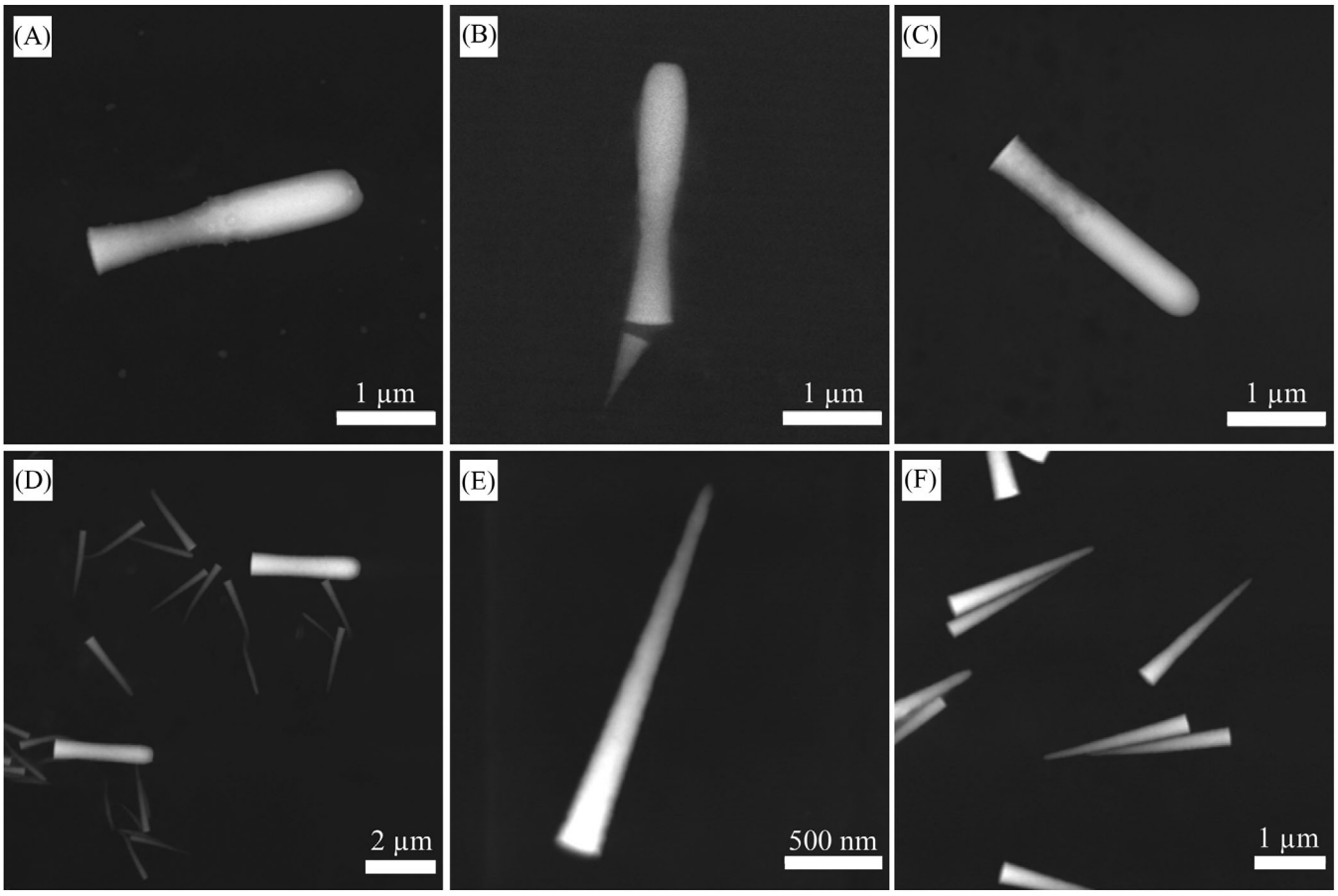

Figure 6 Ex situ etching of silica rod-shaped particles in a basic solution. Particles were attached to the SiN window and placed in a bottle containing 40 mL of (a) 10 mM, and (b) 100 mM NaOH aqueous solutions without stirring. Particles not attached but freely dispersed in a bottle containing 20 mL of (c) 0.5 mM, (d) 3 mM, (e) 10 mM, and (f) 100 mM NaOH solutions. Scale bars indicate 1 μm for (a–d,f), and 500 nm for (e).

mechanism did not take place. Moreover, it was also observed that the ex situ etching at moderate base concentrations such as 3 mM showed both mechanisms with a dependence on the particle size (Figure 6d). We propose that this difference in final shape is due the presence of a higher cross-linked SiO_2 shell around the particle along with the absence of diffusion inside the LC. The shell around the particle becomes thinner going from the rounded tip to the flat end because the exposure time to the growth solution decreases in this direction. Therefore, when the base concentration was high enough it completely etched this silica shell around the particle and etching took place at the tip of the particle at higher etching rates, resulting in a sharper, longer cone-shaped particle. On the other hand, at lower base concentrations only the weakest part of the silica shell etched away and etching continued at the same region by transport of silica from the inner core through the thin shell which caused the particle to break off at this point. The difference between LC etching and ex situ etching where particles undergo free diffusion can be explained by the fact that the particles experience different local NaOH concentrations when they have Brownian motion in the basic solution. In the LC experiments and ex situ control experiments, particles were attached to the SiN window and the etching reaction took place in a diffusion-limited regime. Since the highly cross-linked silica shell was always attached to the SiN window during the whole etching process NaOH always diffused from the weakest part of the shell and etching continued in that region with higher etching rates. However, in the ex situ etching process where the particles diffused freely inside the basic solution the shell around the particle detached at some point due to the self-stirring effect of colloidal particles and etching continued at the tip of the particle with higher etching rates resulting in sharper cone-shaped silica particles. These results reveal that the final shape of the particles can be also tuned by immobilizing them through attachment to a substrate or having them to move freely in the etching solution. However, the higher yields obtainable through bulk etching makes the approach in which the base concentration is optimized for the desired geometries more appealing.

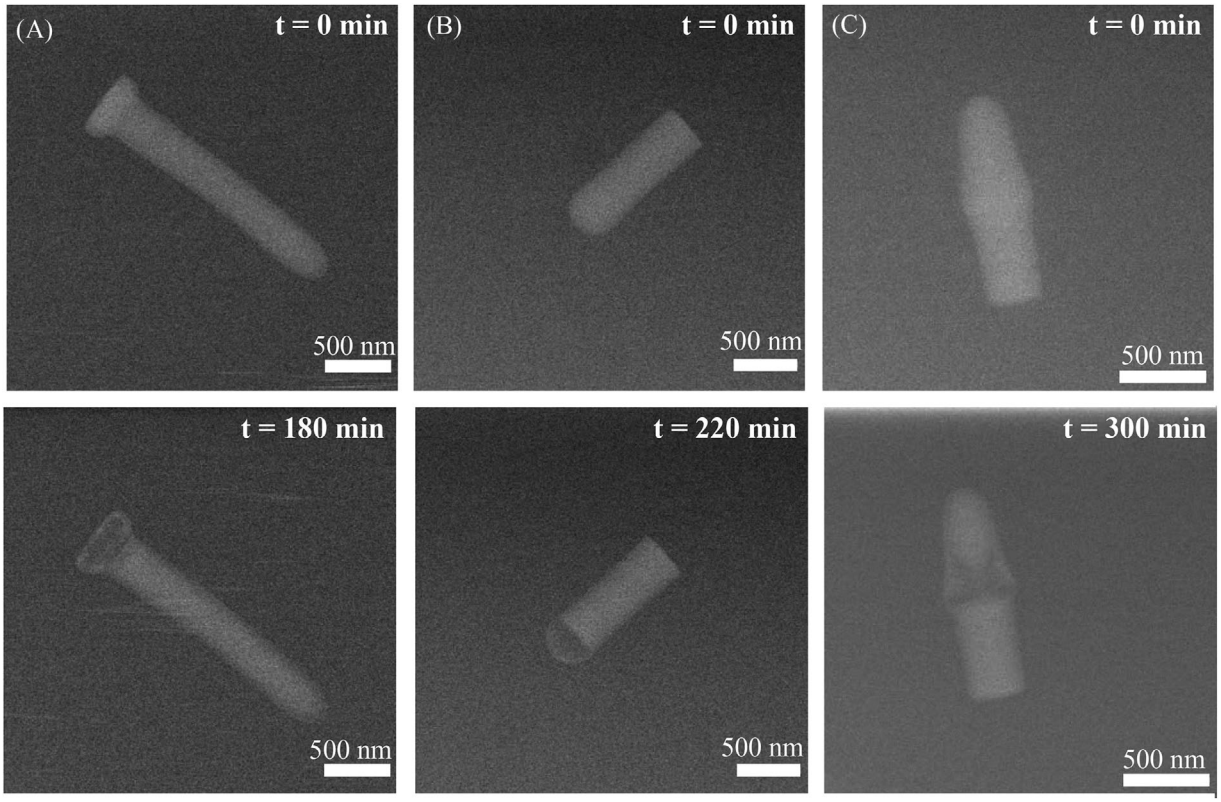

Figure 7 STEM image series of three types of silica rods with different chemical composition and their etched shape with 100 mM NaOH solution using low-dose LC-STEM technique. a) Silica rods consisting of a segment grown at 50 °C followed by a segment grown at 5 °C. b) Silica rods grown at 5 °C followed by a segment grown at 25 °C. c) Silica rods grown subsequently at 25 °C, 5 °C, and 25 °C.[61] The scale bars indicate 500 nm.

2.7 | In situ etching of segmented silica rods

As the last validation for the LC-STEM parameters we have described to perform an in situ silica etching experiments, we analyzed segmented silica rods with a known, even more complex internal inhomogeneous chemical composition by in situ LC etching experiments. Segments of silica rods were grown under different temperature conditions. This adds differences in the internal siloxane condensation degree on top of those already discussed. Varying the temperature influences the degree of condensation of silica. A lower temperature results in a lower degree of condensation with a faster dissolution rate, whereas an increased temperature results in a higher degree of condensation and thus a network that dissolves more slowly.[15,55,59] It is also known that segments silica rods grown at lower temperatures have an increased diameter as the solubility of water in the pentanol oil phase is reduced.[51] Nail-shaped silica rods consisting of a segment grown at 50 °C followed by a segment grown at 5 °C were etched by flowing 100 mM NaOH solution through the LC with these experimental conditions: 0.3 μL min^{-1} flow rate, 4e$^-$ nm^{-2} s^{-1} electron dose rate, and 1.4×10^4 e$^-$ nm^{-2} accumulated electron dose. As expected, etching took place at the less condensed silica segment grown at low temperature even though it was initially thicker, whereas the segment grown at high temperature remained apparently untouched (Figure 7, panel a).[51] As a further illustration, using the same experimental conditions another LC experiment was performed with rods grown at 5 °C followed by a segment grown at 25 °C, and the tip of the particle was preferentially etched as expected (Figure 7, panel b).[51] With a three-step growth of silica rods (25 °C, 5 °C, and 25 °C), silica particles with a thicker but less condensed middle part were synthesized. The in situ etching results for this kind of silica rods are shown in Figure 7, panel c. The LC-STEM observations with the same mentioned experimental conditions agree with the previous results shown by our group[51] for ex situ etching of these particles in bulk, as the middle, less condensed segment etched preferentially. Consequently, the experimental conditions determined in this work for conducting LC-STEM chemical etching experiments of silica rods are applicable to similar systems with a negligible effect of the electron beam as well as of the LC geometry. The high spatial resolution provided by LC-STEM also

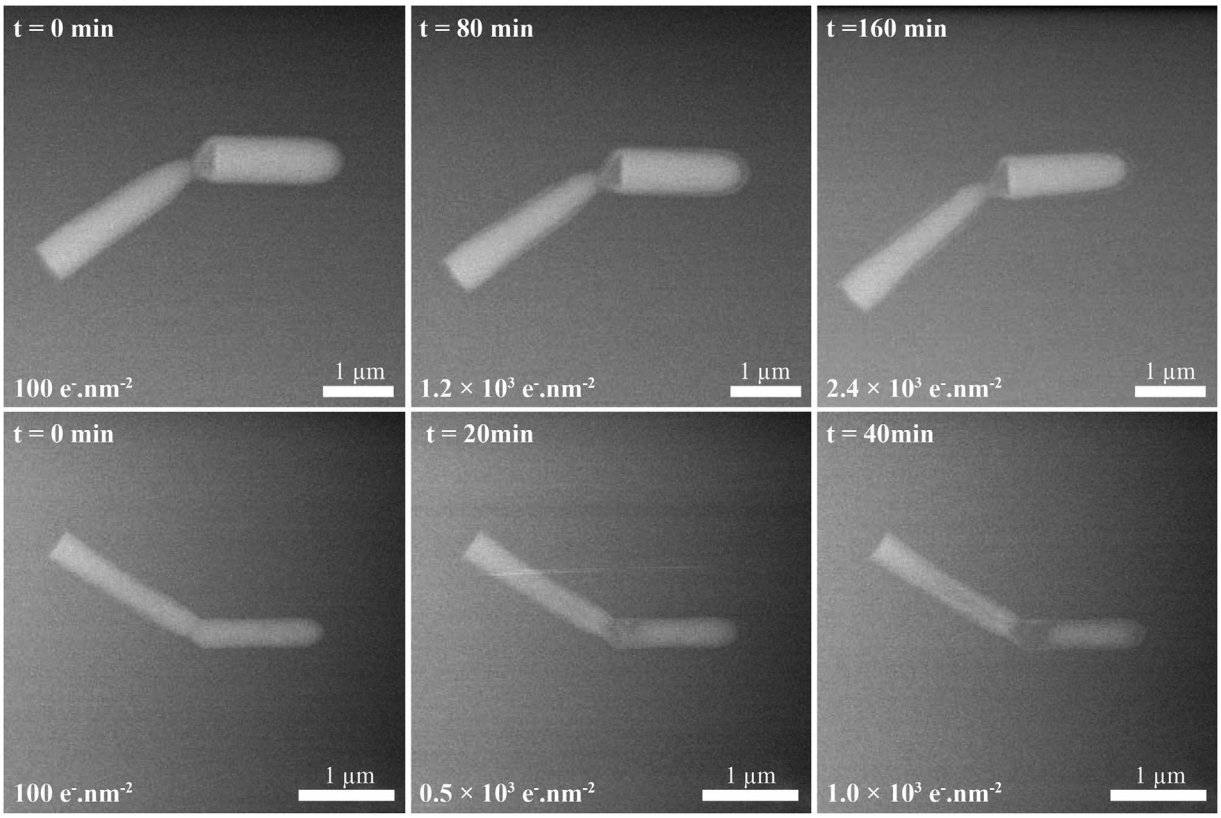

Figure 8 STEM image series of two types of bent silica rods and their etched shape with 100 mM NaOH solution using low-dose LC-STEM technique ($4e^{-}$ nm^{-2} s^{-1}electron dose rate). The corresponding total accumulated electron dose is shown on each frame. a) The bent silica rods that were synthesized at 35 °C with high concentration pre-TEOS. b) The bent silica rods that were synthesized at room temperature using low concentration pre-TEOS. The scale bar indicates 1μm

opens the door to quantifying the etching rates of silica grown at different temperatures. However, the silica rods used in this study consist of a complex internal distribution with different levels of condensation, and thus any measured etching rate would not correspond to that of a particular degree of condensation. We expect that by applying our methodology to simpler silica colloidal particles, future studies will be able to precisely quantify the etching rates of silica of different degrees of condensation.

2.8 | Chemical structure of crooked rod-shaped silica particles

Altering the reaction temperature of the rod-shaped silica particles and/or changing the hydrolysis rate of silica precursor by introducing partially hydrolyzed TEOS (pre-TEOS) into the reaction system results in bending of the rod-shaped silica particles. The synthesis procedure started with synthesizing normal rod-shaped silica particles using standard existing procedures.[16] The reaction was initially carried out above room temperature (35 °C). After one hour of reaction, pre-TEOS was added and the solution was homogenized by shaking for ~1 minute. Five minutes after the addition of pre-TEOS, the reaction mixture was transferred to room temperature for 6–8 hours. As a result, the rods grew into two segments connected at an angle. This reaction can also be carried out at room temperature with lower concentrations of pre-TEOS. For synthesis details on the two types of crooked particles investigated see supplementary information.

Here, we investigated the chemical structure of these two types of crooked silica rods by in situ etching of these particles in basic solutions via LC-STEM. Our results help to better understand the effect of the temperature and the pre-TEOS concentration on the chemical structure of these intriguing particle systems and can be used to tune the bending angle of the two segments, which is important for self-assembly studies.

We applied optimized LC-STEM conditions to study the in situ etching of crooked rod-shaped particles. We flowed 100 mM NaOH solutions with a flow rate of 0.3 $\mu L\,min^{-1}$ and imaged the particles using a 4 $e^{-}\,nm^{-2}\,s^{-1}$ electron dose rate with a total accumulated electron dose below 2.8×10^{3} $e^{-}\,nm^{-2}$. Figure 8 shows the etching of crooked silica rods in time. The particle in panel (a) consists of

two segments; the first segment with a rounded tip was grown at 35 °C while the other segment with a flat end was grown at room temperature. The LC-STEM observations show that the etching of the segment with the flat end occurred faster than the other segment with the round tip. This is expected since the silica grown at elevated temperatures is more condensed compared to the silica which was grown at room temperature.[49] Interestingly no etching was observed at the neck of the particle where the two segments were connected to each other. This can be explained by the fact that adding concentrated pre-TEOS at that point of reaction forms a condensed silica shell around the joint part of the particle which protected it from etching. The particle in panel (b) was grown completely at room temperature using less concentrated pre-TEOS. Although adding pre-TEOS caused the bending of the particle, the two segments were not completely separated. The in situ etching of this particle showed that the least condensed part of the particle was the bending point. The etching was observable at the bent region of the particle approximately 15 minutes after starting to flow the 100 mM NaOH solution. Then etching continued in both sides of the particle indicating the same silica structure of the bent rod-shaped particle. Apparently adding less concentrated pre-TEOS was not enough to protect the bent part of the particle from etching. Moreover, growing at room temperature resulted in particles with a less condensed silica structure that could be easily etched with 100 mM NaOH solution in a short time.

3 | CONCLUSION

We present an optimized LC-STEM method to investigate the etching of micron-sized rod-shaped silica particles in real time and at the single particle level with high spatial resolution. A model system of rod-shaped silica colloidal particles was used to investigate the etching mechanism of these particles in basic conditions. By utilizing low-dose electron beam conditions and by optimizing the flow-rate of the NaOH solutions during the LC-STEM observations, we showed that investigation of the etching of rod-shaped silica particles is attainable with a negligible effect of the electron beam irradiation if also the total dose is kept below 3.4×10^4 $e^- nm^{-2}$ by only taking a limited number of images. LC-STEM observations revealed that the base-induced etching occurs inhomogeneously along the length of the rod due to its inhomogeneous chemical structure. Remarkably, the LC-STEM observations revealed a three-step etching mechanism which transformed the rod-shaped silica particles into cone-shaped silica particles. The mechanism started with etching at a region in the middle of the particle closer to the flat end, which is the most etchant-sensitive part of the particle. The etching then continued at a faster rate at the sensitive part of the particle and finally necking-and-breaking occurred at the same point of the particle which yielded a cone-shaped silica particle. Comparison between the LC and the ex situ etching experiments suggests that the geometry of the LC plays a significant role in chemical reactions where diffusion of reactants and/or particles are important, and that with the current equipment for LC experiments the reactions studied in this paper were in a diffusion-limited regime. The optimized LC-STEM conditions were further tested by utilizing a new class of silica rod-shaped particles where the chemical structure of the rod was tailored deliberately. The etching of segmented silica rods happened as was expected, validating the LC-STEM optimized conditions found in this work. Finally, using optimized LC-STEM conditions we revealed the chemical composition of the recently developed rod-shaped silica particles known as crooked silica rods. We expect that using similar low-dose imaging conditions and optimized flow-rates of solutions as determined in this work, will allow for investigations of chemical reactions with colloids using the LC-STEM technique with negligible effects of the electron beam, and will thus serve as a powerful new technique to probe the evolution of etching at the single particle level. Furthermore, we are confident that, although the imaging conditions w.r.t. dose rates and accumulated doses were only possible with the relatively large particles used, future and ongoing improvements of detectors and smart imaging routines will strongly push down the size and structures that can be imaged without major interference from the imaging itself! Especially, not taking continuous movies, but just a few frames is often enough to still obtain the necessary information.

4 | EXPERIMENTAL SECTION

4.1 | In situ liquid cell etching experiments

A Hummingbird Scientific (USA) Liquid Cell dedicated holder was used to perform the in situ experiments. A Hamilton syringe pump equipped with a 1 mL glass syringe was used to flow solutions through the microfluidic tubing into the cell. To flow the 400 nm spherical particles, for measuring the flow velocity, a diluted suspension of the nanoparticles was loaded into the syringe and flowed into the cell. Silicon chips with SiN windows (50 × 200 μm × 50 nm thickness) were used to encapsulate the liquid volume. In all experiments, 2 μm spacers were used between top and bottom chips. The sample preparation started with glow discharging of the side of the chips which was in contact with liquid for 90 seconds to make them hydrophilic.

2 μL of diluted sample with a volume fraction of 21 g L^{-1} was drop-casted on the top chip and allowed to dry. This ensured that a number of particles were attached to the top window, where the STEM resolution for LC experiment is the highest. Next, the bottom chip was placed in the dedicated holder and 2 μL of deionized water was drop-casted onto it to ensure that the cell contained liquid, after which the top chip was placed in position.

4.2 | Ex situ etching experiments

Ex situ etching of silica rods was carried out as follows. For the experiment on freely dispersed particles the sample volume fraction was fixed at 21 g L^{-1} (350 mmol L^{-1}) and 575 μL of this sample in ethanol was redispersed in 20 mL of the desired concentration of aqueous NaOH (reagent grade, ≥98%, pellets, Sigma-Aldrich) in plastic vials. For the concentrations 100 and 10 mM NaOH samples were collected every 15 minutes for 8 hours. For the concentration 3 mM NaOH samples were collected every 1 hour for 8 hours and 2 final samples were collected after 20 and 24 hours. For the 0.50 mM NaOH concentration samples were collected every 1 hour for 8 hours and 3 final samples were collected after 24, 48, and 72 hours. All samples were prepared by drop-casting 5 μL of the sample solution on a Formvar/Carbon Film 200 Mesh Copper TEM grid. The grids were dried under a heating lamp to quickly stop the etching reaction on the grid.

For ex situ experiments where the particles were attached to a SiN membrane of the LC chip the sample volume fraction was fixed at 21 g L^{-1} and 2 μL of this sample was drop-casted on the LC chip and allowed to dry. The chip was then placed in a plastic vial containing 40 mL of the desired concentration of aqueous NaOH. The vials were left to stand on the table without stirring. The experiments were carried out with 100 mM and 10 mM NaOH concentrations. Samples were collected every 15 minutes for 8 hours and for each time interval a separate SiN chip was utilized.

All LC-STEM experiments and STEM measurements were carried out with a Tecnai-F20 transmission electron microscope (TEM, Thermo Fisher Scientific) equipped with a field emission gun and operating at 200 keV using an annular dark-field detector (ADF, E.A. Fischione Instruments Inc., Model 3000, USA) with a camera length of 120 mm. The dose rate was calculated from the beam current of the empty column (no holder) and the frame size as follows:[60]

$$d = \frac{I_e}{eA} \tag{5}$$

Here d is the electron dose rate, I_e is the beam current, e is the elementary charge, and A is the total frame size determined by the magnification.

ACKNOWLEDGMENTS

S.S. and A.G. contributed equally to this work. This project has received funding from the NWO-TTW Perspectief Program 'Understanding Processes Using Operando Nanoscopy', project UPON-B3 (no. 14206). We also acknowledge funding from the European Research Council (ERC) via the ERC Consolidator Grant NANO-INSITU (grant no. 683076). R.K. acknowledges funding from the Netherlands Center for Multiscale Catalytic Energy Conversion (MCEC), an NWO Gravitation programme funded by the Ministry of Education, Culture, and Science of the government of the Netherlands. F.H. acknowledges funding from the Netherlands Organisation for Scientific Research (NWO).

REFERENCES

1. S. C. Glotzer, M. J. Solomon, *Nat. Mater.* **2007**, *6*, 557.
2. S. M. Yang, S. H. Kim, J. M. Lim, G. R. Yi, *J. Mater. Chem.* **2008**, *18*, 2177.
3. A. Perro, S. Reculusa, S. Ravaine, E. Bourgeat-Lami, E. Duguet, *J. Mater. Chem.* **2005**, *15*, 3745.
4. G. J. Vroege, H. N. W. Lekkerkerker, *Rep. Prog. Phys.* **1992**, *55*, 1241.
5. M. Bär, R. Großmann, S. Heidenreich, F. Peruani, *Annu. Rev. Condens. Matter Phys* **2020**, *11*, 441.
6. C. J. Murphy, A. M. Gole, S. E. Hunyadi, J. W. Stone, P. N. Sisco, A. Alkilany, B. E. Kinard, P. Hankins, *Chem. Commun.* **2008**, 544.
7. S. Y. Zhang, M. D. Regulacio, M. Y. Han, *Chem. Soc. Rev.* **2014**, *43*, 2301.
8. K. Thorkelsson, P. Bai, T. Xu, *Nano Today* **2015**, *10*, 1.
9. A. S. Sonin, N. A. Churochkina, A. V. Kaznacheev, A. V. Golovanov, *Colloid J.* **2017**, *79*, 421.
10. F. Li, D. P. Josephson, A. Stein, *Angew. Chem. Int. Ed.* **2011**, *50*, 360.
11. A. van Blaaderen, *Nature* **2006**, *439*, 545.
12. S. Sacanna, D. J. Pine, G. R. Yi, *Soft Matter* **2013**, *9*, 8096.
13. A. Kuijk, A. Imhof, M. H. W. Verkuijlen, T. H. Besseling, E. R. H. van Eck, A. van Blaaderen, *Part. Part. Syst. Charact.* **2014**, *31*, 706.
14. J. W. Park, Y. J. Park, C. H. Jun, *Chem. Commun.* **2011**, *47*, 4860.
15. A. van Blaaderen, A. P. M. Kentgens, *J. Non-Cryst. Solids* **1992**, *149*, 161.
16. A. Kuijk, A. van Blaaderen, A. Imhof, *J. Am. Chem. Soc.* **2011**, *133*, 2346.
17. A. Kuijk, D. V. Byelov, A. V. Petukhov, A. van Blaaderen, A. Imhof, *Faraday Discuss.* **2012**, *159*, 181.
18. A. Kuijk, T. Troppenz, L. Filion, A. Imhof, R. van Roij, M. Dijkstra, A. van Blaaderen, *Soft Matter* **2014**, *10*, 6249.
19. F. Hagemans, E. B. van der Wee, A. van Blaaderen, A. Imhof, *Langmuir* **2016**, *32*, 3970.
20. N. de Jonge, F. M. Ross, *Nat. Nanotechnol.* **2011**, *6*, 695.

21. F. M. Ross, *Science* **2015**, *350*, 6267.
22. H. Wu, H. Friedrich, J. P. Patterson, N. A. J. M. Sommerdijk, N. de Jonge, *Adv. Mater.* **2020**, *32*, 2001582.
23. N. M. Schneider, M. M. Norton, B. J. Mendel, J. M. Grogan, F. M. Ross, H. H. Bau, *J. Phys. Chem. C* **2014**, *118*, 22373.
24. P. Abellan, T. J. Woehl, L. R. Parent, N. D. Browning, J. E. Evans, I. Arslan, *Chem. Commun.* **2014**, *50*, 4873.
25. T. J. Woehl, K. L. Jungjohann, J. E. Evans, I. Arslan, W. D. Ristenpart, N. D. Browning, *Ultramicroscopy* **2013**, *127*, 53.
26. T. A. J. Welling, S. Sadighikia, K. Watanabe, A. Grau-Carbonell, M. Bransen, D. Nagao, A. van Blaaderen, M. A. van Huis, *Part. Part. Syst. Charact.* **2020**, *37*, 2070014.
27. T. J. Woehl, P. Abellan, *J. Microsc.* **2017**, *265*, 135.
28. Y. Jiang, G. Zhu, F. Lin, H. Zhang, C. Jin, J. Yuan, D. Yang, Z. Zhang, *Nano Lett.* **2014**, *14*, 3761.
29. H. Liao, L. Cui, S. Whitelam, H. Zheng, *Science* **2012**, *336*, 1011.
30. J. M. Yuk, J. Park, P. Ercius, K. Kim, D. J. Hellebusch, M. F. Crommie, J. Y. Lee, A. Zettl, A. P. Alivisatos, *Science* **2012**, *336*, 61.
31. M. Piffoux, N. Ahmad, J. Nelayah, C. Wilhelm, A. Silva, F. Gazeau, D. Alloyeau, *Nanoscale* **2018**, *10*, 1234.
32. R. G. Weiner, D. P. Chen, R. R. Unocic, S. E. Skrabalak, *Small* **2016**, *12*, 2701.
33. J. H. Park, N. M. Schneider, J. M. Grogan, M. C. Reuter, H. H. Bau, S. Kodambaka, F. M. Ross, *Nano Lett.* **2015**, *15*, 5314.
34. K. L. Jungjohann, S. Bliznakov, P. W. Sutter, E. A. Stach, E. A. Sutter, *Nano Lett.* **2013**, *13*, 2964.
35. S. F. Tan, G. Lin, M. Bosman, U. Mirsaidov, C. A. Nijhuis, *ACS Nano* **2016**, *10*, 7689.
36. T. J. Woehl, J. E. Evans, I. Arslan, W. D. Ristenpart, N. D. Browning, *ACS Nano* **2012**, *6*, 8599.
37. L. R. Parent, E. Bakalis, A. Ramírez-Hernández, J. K. Kammeyer, C. Park, J. De Pablo, F. Zerbetto, J. P. Patterson, N. C. Gianneschi, *J. Am. Chem. Soc.* **2017**, *139*, 17140.
38. J. Hermannsdörfer, N. de Jonge, A. Verch, *Chem. Commun.* **2015**, *51*, 16393.
39. G. Zhu, Y. Jiang, F. Lin, H. Zhang, C. Jin, J. Yuan, D. Yang, Z. Zhang, *Chem. Commun.* **2014**, *50*, 9447.
40. K. W. Noh, Y. Liu, L. Sun, S. J. Dillon, *Ultramicroscopy* **2012**, *116*, 34.
41. T. Kraus, N. Jonge, *Langmuir* **2013**, *29*, 8427.
42. J. P. Patterson, P. Abellan, M. S. Denny, C. Park, N. D. Browning, S. M. Cohen, J. E. Evans, N. C. Gianneschi, *J. Am. Chem. Soc.* **2015**, *137*, 7322.
43. P. Abellan, T. H. Moser, I. T. Lucas, J. Grate, J. E. Evans, N. D. Browning, *RSC Adv.* **2017**, *7*, 3831.
44. Z. Aabdin, X. M. Xu, S. Sen, U. Anand, P. Král, F. Holsteyns, U. Mirsaidov, *Nano Lett.* **2017**, *17*, 2953.
45. K. Y. Niu, J. Park, H. Zheng, A. P. Alivisatos, *Nano Lett.* **2013**, *13*, 5715.
46. S. W. Chee, S. F. Tan, Z. Baraissov, M. Bosman, U. Mirsaidov, *Nat. Commun.* **2017**, *8*, 1.
47. Z. Zeng, X. Zhang, K. Bustillo, K. Y. Niu, C. Gammer, J. Xu, H. Zheng, *Nano Lett.* **2015**, *15*, 5214.
48. T. H. Moser, H. Mehta, C. Park, R. T. Kelly, T. Shokuhfar, J. E. Evans, *Sci. Adv.* **2018**, *4*, eaaq1202.
49. C. Brinker, *J. Non-Cryst. Solids* **1988**, *100*, 31.
50. R. K. Iler, *The Chemistry of Silica: Solubility, Polymerization, Colloid and Surface Properties, and Biochemistry*, Wiley, New York **1979**.
51. F. Hagemans, W. Vlug, C. Raffaelli, A. van Blaaderen, A. Imhof, *Chem. Mater.* **2017**, *29*, 3304.
52. F. Hagemans, R. K. Pujala, D. S. Hotie, D. M. Thies-Weesie, D. A. de Winter, J. D. Meeldijk, A. van Blaaderen, A. Imhof, *Chem. Mater.* **2019**, *31*, 521.
53. Y. Yang, G. Chen, L. J. Martinez-miranda, H. Yu, K. Liu, Z. Nie, *JACS* **2016**, *138*, 68.
54. Y. Yang, H. Pei, G. Chen, K. T. Webb, L. J. Martinez-Miranda, I. K. Lloyd, Z. Lu, K. Liu, Z. Nie, *Sci. Adv.* **2018**, *4*, 5.
55. C. J. Brinker, R. Sehgal, S. L. Hietala, R. Deshpande, D. M. Smith, D. Loy, C. S. Ashley, *J. Membr. Sci.* **1994**, *94*, 85.
56. M. W. P. van de Put, C. C. M. C. Carcouët, P. H. H. Bomans, H. Friedrich, N. de Jonge, N. A. J. M. Sommerdijk, *Small* **2015**, *11*, 585.
57. S. Broersma, *J. Chem. Phys.* **1960**, *32*, 1632.
58. M. M. Tirado, C. L. Martínez, J. García, D. Torre, *J. Chem. Phys.* **1984**, *81*, 2047.
59. Y. J. Wong, L. Zhu, W. S. Teo, Y. W. Tan, Y. Yang, C. Wang, H. Chen, *J. Am. Chem. Soc.* **2011**, *133*, 11422.
60. A. Verch, M. Pfaff, N. de Jonge, *Langmuir* **2015**, *31*, 6956.
61. M. Kamp, G. Soligno, F. Hagemans, B. Peng, A. Imhof, R. van Roij, A. van Blaaderen, *J. Phys. Chem. C* **2017**, *121*, 19989.

SUPPORTING INFORMATION

Additional supporting information may be found online in the Supporting Information section at the end of the article.

How to cite this article: Sadighikia S, Grau-Carbonell A, Welling TAJ, et al. Low-dose liquid cell electron microscopy investigation of the complex etching mechanism of rod-shaped silica colloids. *Nano Select*. 2021;2:313–327. https://doi.org/10.1002/nano.202000060